Surface Science 631 (2015) 23–34

Contents lists available at ScienceDirect

Surface Science

journal homepage: www.elsevier.com/locate/susc

Underpotential deposition: From planar surfaces to nanoparticles

O.A. Oviedo [a], P. Vélez [a], V.A. Macagno [b], E.P.M. Leiva [a,*]

[a] Instituto de Investigaciones de Fisicoquímica de Córdoba (INFIQC — CONICET), Departamento de Matemática y Física, Facultad de Ciencias Químicas, Universidad Nacional de Córdoba, X5000HUA Córdoba, Argentina
[b] Instituto de Investigaciones de Fisicoquímica de Córdoba (INFIQC — CONICET), Departamento de Fisicoquímica, Facultad de Ciencias Químicas, Universidad Nacional de Córdoba, X5000HUA Córdoba, Argentina

ARTICLE INFO

Available online 19 August 2014

Keywords:
Underpotential deposition
Nanothermodynamic
Co-adsorption
Electrodeposition

ABSTRACT

An overview is given of selected theoretical, experimental and computer simulation research on thermodynamic modeling applied to the metal underpotential deposition. Focus is made mainly on the last 20 years. The *upd*-theory on planar surfaces is revisited and the thermodynamic framework is extended to consider underpotential deposition on nanoparticles and to include anion coadsorption, solvation and double layer charging. Results from molecular dynamics and Monte Carlo simulations are shown for systems of experimental interest. At the end some perspectives for further advanced modeling of the present problem are given.

© 2014 Elsevier B.V. All rights reserved.

1. Introduction

1.1. 20 years of progress in underpotential deposition. General aspects

The last two decades have witnessed major advances in the characterization and development of a new generation of nano- and molecular devices. Nanoscience and nanotechnology have been the branches of science dealing with these systems. The main purpose of nanotechnology is the manufacture, manipulation and integration of nanoscale devices in order to obtain products with novel physicochemical properties, and nanoscience is providing the basic support for these achievements. Manufacture of items in this scale can be accomplished via two strategies: a (so as to say) conventional manufacturing, starting from large objects going down to progressively smaller ones (also called top-down) and a molecular manufacturing (also called bottom-up). The first is the strategy that has characterized the innovations of the last century, while the second is expected to predominate in the present century [1]. Today we are facing a transitional stage between these two strategies.

In the bottom-up strategy, tiny individual parts are linked together to form larger components with a higher hierarchy, which in turn are linked with each other to form a larger system, and so on. This mechanism has been inspired by nature as it happens, for example, with the assembly of a protein. The central idea in this strategy is to manipulate the reaction conditions and interaction forces to obtain controlled growth of the desired structure at will, so that the building blocks self-assemble and the desired product is obtained. Addressing the growth mechanism of such structures is not an easy task and this constitutes a source for new challenges and paradigms. A wide variety of building blocks exists, such as fullerenes, nanotubes, DNA, quantum dots, dendrimers, copolymers, and nanoparticles. Currently, joint efforts between different branches of science are undertaken in order to find better synthetic strategies and to improve the kinetic and thermodynamic stability of the resulting structures or devices. Thanks to these efforts, our understanding of the processes involved in the formation of nanostructures at the atomistic level has increased considerably in the last 20 years. This has been possible in part through the development and improvement of experimental techniques such as scanning tunneling microscopy, electron microscopy and those derived from synchrotron light. Nowadays, it is possible to monitor the behavior of a small set of atoms or even a single molecule directly and in real time. On the other hand, our knowledge in the area has improved thanks to the development of theoretical models and computational techniques. The development of information technology has generated more computing power, which has increased concomitantly with the size of the hardware. It is possible today to compare experimental measurements with an atomistic view generated from a molecular simulation. This synergy allows the validation (and/or refinement) of models and can even contribute to the development of new synthetic strategies in a more accurate, efficient and faster way than in the previous decades.

Getting into the electrochemical field, it comes out that various strategies, originally used for the modification of flat surfaces, are nowadays successfully applied to design and modify nano-sized structures. Among these, the modification of a metal surface by underpotential deposition (*upd*) is of great interest, which consists in metal deposition on a foreign substrate at potentials positive with respect to the Nernst thermodynamic prediction. Although it sounds awkward, the term *upd* was developed to mark the contrast with the current metal deposition, which always involves an overpotential deposition (*opd*) due to kinetic hindrances. The potential utility of *upd* is due to the relatively rapid, simple and precise modification of the reaction conditions, which allow controlling the degree of coverage of the adsorbate metal on the substrate surface. The

* Corresponding author.
E-mail address: eze_leiva@yahoo.com.ar (E.P.M. Leiva).

http://dx.doi.org/10.1016/j.susc.2014.08.020
0039-6028/© 2014 Elsevier B.V. All rights reserved.

main obstacle to the implementation of *upd* for a large number of systems is the fact that this phenomenon is limited in many cases to the deposition of a less noble metal on a more noble one. In the case of electrocatalytic applications, this situation is right the opposite of the desired one. One way to circumvent this problem is to use a technique that denominated galvanic replacement (*gr*). In this method, the substitution of a sacrificial *upd* sub/monolayer by the desired noble metal atop in circuit allows obtaining the desired catalyst. Applied together, *upd* and *gr* allow reducing the quantity of noble metal used to a minimum amount, thus reducing the economic costs of the final product. This is a key objective for potential industrial applications. Thus, both *upd* and *gr* appear as attractive bottom-up methods, with great prospects for the development of novel nanomaterials. The contribution of the present work is directed to discuss research on some basic aspects of *upd* that have brought new insight into this phenomenon in the last two decades.

1.2. Overview on recent experimental and theoretical progress

Although there is not currently a book exclusively devoted to the discussion of *upd* phenomena, there are various review articles [2,3,62] and book chapters on it [4–12]. The present article is not intended to summarize all the work in the field, but rather to focus the discussion on some recent advances on this phenomenon, especially concentrating on the theoretical point of view in the last two decades.

The formation of core@shell structures may be considered as the nano-counterpart of heterogeneous metal growth on planar foreign substrates. While in the latter case the occurrence of overpotential and underpotential deposition phenomena is well known and there are whole books devoted to their analysis [4], the possibility of occurrence of *upd* and *opd* on nanoparticles has been rather seldom mentioned in the literature and its theoretical analysis dates back to 2008. Concerning experiments, Selvakannan et al. [13] showed in 2004 that tyrosine molecules used as surface stabilizers of Au NPs may also reduce Ag ions present in the electrolyte solution to yield core@shell NPs of the type Au@Ag. The protonation of the phenolic group of tyrosine, which is responsible for its reductive ability, was found to be controlled via the *p*H of the solution, thus allowed tuning the reductive power of this molecule. Fonticelli et al. showed in 2007 [14] that p-benzoquinone (a molecule with similar characteristics to those of tyrosine) can be used to reduce Ag ions on the surface of a Au-NP coated with thiol molecules. The main difference between the experiments of Selvakannan et al. and those of Fonticelli et al. is that in the first case the reducing molecules were on the surface of the NP, while in the second they were free in solution. This is a slight but significant difference, since the reducing molecules on the surface of the NP may be influenced by the presence of a second material, thereby affecting the deposition process. The final results of the synthesis of Fonticelli et al. were Au@Ag thiol stabilized NPs. This work also showed that the electric potential for metal deposition on a NP freely suspended in solution can be tuned using molecules with acid–base activity, in very much the same way that a potentiostat is used to control the surface potential of an electrode. Thus, in this picture, the NP resembles a nanoelectrode that can be wired to a desired potential via a redox system. However, here the question arises concerning the similarities and the differences between an infinitely large electrode and a NP used as electrode. Wood and Plieth [15–17] tackled this problem already in the '80s. Wood noted that the work function, that is, the work to extract an electron right outside the surface a NP of radius *r* is given by:

$$\Phi^{NP} = \Phi^{bulk} + \frac{3}{8}\left(\frac{e_0^2}{r}\right) \quad (1)$$

where Φ^{bulk} is the work function of the bulk material ($\Phi^{bulk} > 0$) and e_0 corresponds to the elementary charge. The second term on the *rhs* of Eq. (1) is always positive, indicating that $\Phi^{NP} > \Phi^{bulk}$ for a finite *r*. In this way, extracting an electron from a NP always involves a larger work than taking it out from the corresponding bulk material and this work will become larger the smaller the NP. Thus, this early work showed that curvature effects may become important in electrochemical processes where the work function is known to play a relevant role, like for example determining the potential of zero charge of the electrode. However, the relevance of NP size for *upd* had to wait much longer to be considered.

In 2008 Leiva and coworkers [18,19] modified the existing *upd* thermodynamic framework to consider the process of electrochemical deposition in systems with curvatures at the nanometric level. This development, based on nanothermodynamic concepts developed by Hill [20] allowed the study of new scenarios for *upd* at the nanoscale. The new modeling anticipated novel behaviors for nanosystems: in those with negative curvatures, such as nanocavities, *upd* should be favored, while in those with positive curvatures such as NPs, the opposite should occur. Following these ideas, Oviedo et al. [19,63–65] used computer simulations to study the process of Ag *upd* on Au-NPs and found that this phenomenon could reach a limit for small NPs. Something similar should happen for Pd deposition on Au-NPs [21]. Then, Comptom and coworkers [22–24] showed experimental evidence indicating that the *upd* phenomenon could disappear in the case of deposition of Pb and Cd on Ag-NPs of relatively small size. The occurrence of a *upd–opd* transition is of great relevance, since this would set a limit to bottom-up layer-by-layer techniques [25,12].

One of the behaviors observed at the nanoscale that has no counterpart on single crystal flat surfaces is the selective decoration of the facets of a NP. It is known that on flat surfaces *upd* is more prone to occur on open surfaces. Thus, a proper choice of the deposition potential enables deposition at the more open facets of a NP. This effect has been used to block (or promote) growth on these facets and thereby control crystal growth. This strategy has been employed in the Ag/Au system [26,27] to get a variety of NP shapes.

Upd may be strongly modified by anion coadsorption [66]. Electronic structure calculations indicate that the coadsorption of sulfate plays a key role in making possible *upd* Cu on Au(111) [28] and something similar happens with Cu deposition of Pt-NPs [29]. Langille et al. [30] have analyzed in detail the effect of including other anions like chloride, bromide and iodide in NP growth under *upd* control. On the other hand, Tran and Lu [31] have analyzed the effect of the presence of Pd and Ag ions on Au NP growth. Overall, this strategy allows obtaining NPs with high index facets, as well as NPs with concave facets that are very important for technological applications in electrocatalysis.

As mentioned above, one of the main handicaps of *upd* is the need to deposit a less noble metal on another more noble one. One way to circumvent this problem is to produce a galvanic replacement, where the *upd* sub/monolayer is used as a sacrificial deposit [32–34]. Thus, the successive use of *upd* and *gr* allows synthesizing nanomaterials with a minimal use of precursors, lowering the end cost of the product [35]. Inclusion of a third metal and/or performing several *upd–gr* cycles allows the construction of complex sandwich structures, which exhibit properties different from those of the separated materials [36].

Recent progress has also been made in determining the various thermodynamic contributions to the *upd* process. Some studies based on the lattice gas have analyzed the configurational entropic contributions in comparison with the energetic ones [3]. These studies have demonstrated that the formation of the bond between the adsorbate and the substrate, that is, the potential energy of the metal interactions, delivers the main contribution to *upd*. The latter has been confirmed for pseudomorphic systems, where atomistic computer simulations have shown that the contribution of vibrational entropy to *upd* does not exceed 5% [37]. Conway and Chacha [38] have studied experimentally the entropic contributions to Pb-*upd* on polycrystalline Au, on the basis of the analysis of the change of the *upd* shift [44–46] with temperature. From their measurements, they estimated entropic contributions to *upd* shift ranging between 185 and 307 mV. Taking into account that the *upd* shift estimated in Ref [39] for Pb deposition on Au(111) is 215 mV, the values of

Conway and Chacha indicate that entropy would play an essential role in determining Pb-*upd* on Au(111). Farigliano et al. [40] have recently tackled this problem by means of theoretical tools. Using the two-phase model developed by the Goddard and coworker (2PT) [41,42], these authors decomposed the entropic contributions into translational and vibrational. These studies showed that the vibrational contributions amount a 20% of the *upd* shift of the Pb monolayer deposited on Au (111), the remaining 80% stemming from energetic contributions. These results show that in the case of non-pseudomorphic systems entropic contributions may become important and should be taken into account when estimating the relative stability of different *upd* phases.

In the following sections we present an overview on some of the most recent advances in the theoretical field of *upd*. We start analyzing a simple model for *upd* on planar surfaces. Then, we present a derivation for thermodynamic modeling of *upd* considering coadsorption, solvation and double layer charging. Finally, we discuss the modeling of adatom adsorption on nanoparticles, considering the possibility of *upd–opd* transitions. While in Sections 2 and 4 we revisit previous work in a comprehensive view, the modeling presented in Section 3 is completely new.

2. A simple approach to underpotential deposition on flat surfaces

Fig. 1 shows a diagram of an electrochemical system used to measure the *upd* on a bulk electrode, which for practical purposes may be assumed to have an infinite surface. The entire electrochemical system consists of a subsystem (enclosed by dotted line) and two electron reservoirs, which are connected electronically to the electrodes through metal leads. The subsystem contains the electrochemical cell, namely the two electrodes and the electrolyte. The electrode of the left, chosen to be the working electrode (W) is constructed from a bulk piece of metal S. The right electrode, is a reference one (R) built from a bulk piece of metal M. All phases present in the subsystem are considered large enough so that their properties can be deduced from macroscopic thermodynamics. The dotted line surrounding the subsystem indicates that matter exchange with the environment is precluded with the exception of electrons. The temperature and pressure of the subsystem are controlled by two infinite reservoirs (not shown). The system is assumed to be in equilibrium, so that at the potential difference applied no net reaction occurs. In the following paragraphs we discuss the transfer of an ion core from the R to the W electrode under equilibrium conditions.

The oxidation reaction of an M atom at the R electrode may be written as:

$$M \rightarrow M^{z+} + z e_R^- \tag{2a}$$

where e_R^- corresponds to the electrons generated in the reaction, and z is the charge of the metal cation M^{+z}. To keep electroneutrality at the R electrode, z electrons generated in reaction (2a) flow to the reservoir at the electrochemical potential $\tilde{\mu}_e^M$, while the cation migrates through the electrolyte solution to the other electrodes. Upon arriving at the S electrode, the M^{z+} cation is assumed to completely discharge on the working electrode W, joining a monolayer of M on the surface of S. This reaction may be written:

$$M^{z+} + S + z e_M^- \rightarrow M/S \tag{2b}$$

where the e_M^- electrons are taken from the W electrode. These electrons flow from the reservoir at the electrochemical potential $\tilde{\mu}_e^S$. The addition of reactions (2a) and (2b) result in:

$$M + S + z e_M^- \rightarrow M/S + z e_R^- \tag{2c}$$

where we have written explicitly the source and sink of the electrons in reactions (2a) and (2b). In the following we omit this feature. We can see that reaction (2c) represents nothing but the transfer of a M atom from the bulk of the M material to the monolayer of M adsorbed on S, with the corresponding electronic flow at the electrodes to keep charge neutrality. As stated above, the electrodes are connected to respective electronic reservoirs with fixed electrochemical potentials of electrons $\tilde{\mu}_e^S$ and $\tilde{\mu}_e^M$. Since the electrodes have respectively attached two pieces of a metal of the same chemical nature M_2, we can replace the difference of electrochemical potentials $\Delta\tilde{\mu}_e = \left(\tilde{\mu}_e^S - \tilde{\mu}_e^M\right)$ by the difference of Volta potentials $e_0(\psi^M - \psi^S)$.

From a thermodynamic viewpoint, it appears at first sight that the electrochemical cell (subsystem) given in Fig. 1 could be described in terms of the variables $N_{M^{z+}}, N_S, P$ and T. If this was the case, the thermodynamic magnitude predicting the stability of this subsystem would be the free Gibbs energy G^{sub}. However, the cell is actually an open system with respect to the electrons, which may freely flow between it and the

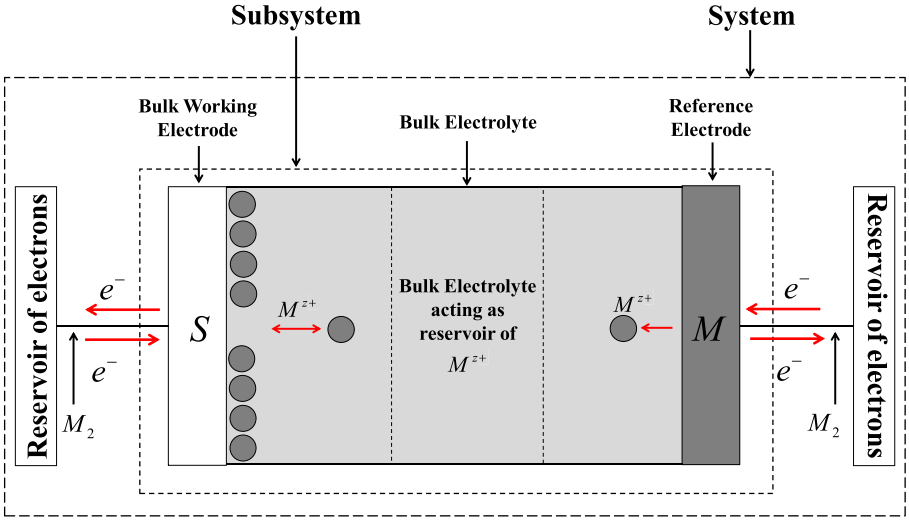

Fig. 1. Scheme of an electrochemical system is used to measure underpotential shift. The dotted line encloses the subsystem containing the electrodes and the electrolyte. This subsystem is only open for electrons, which may freely flow between it and the reservoirs through the wires made of metal M_2.

electronic reservoirs, where the electrochemical potentials of the electrons are assumed to be fixed. Thus, it is necessary to define a new thermodynamic potential considering this situation. Let us denote it with $\widetilde{G}$, which corresponds to a Legendre transformation of G^{sub} according to:

$$\widetilde{G} = G^{sub} - N_e^S \widetilde{\mu}_e^S - N_e^M \widetilde{\mu}_e^M \tag{3}$$

where N_e^S and N_e^M correspond to the number of electrons present at the W and R electrodes, respectively. Then, the change of the transformed free energy $\Delta\widetilde{G}$, as a consequence of the deposition of N_M atoms may be written as:

$$\Delta\widetilde{G} = \Delta G^{sub} - \Delta N_e^S \widetilde{\mu}_e^S - \Delta N_e^M \widetilde{\mu}_e^M \tag{4}$$

where ΔN_e^S and ΔN_e^M correspond to the change of the number of electrons in each electrode involved in reaction (2c). The next step is to write Eq. (4) in terms of $N_{M^{z+}}$, the number of atoms of type M being deposited on S. This can be done using the restrictions imposed by Eqs. (2a)–(2c). With the assumptions made, we have:

- $\Delta N_e^S + \Delta N_e^M = 0$ and,
- $N_{M^{z+}} = z\Delta N_e^M$.

From this, Eq. (4) may be written as:

$$\Delta\widetilde{G} = \Delta G^{sub} + N_{M^{z+}}\left(\widetilde{\mu}_e^M - \widetilde{\mu}_e^S\right). \tag{5a}$$

Taking into account that the electrochemical potential of electrons in a metal i is defined by:

$$\widetilde{\mu}_e^i = \mu_e^i - e_0\psi^i \tag{5b}$$

where ψ^i is the internal potential of the metal phase and considering that the reservoirs are connected by the same metal M_2, we get:

$$\Delta\widetilde{G} = \Delta G^{sub} + ze_0 N_{M^{z+}}\eta \tag{5c}$$

where we have replaced the difference of Volta potentials by the overpotential, $(\psi_S - \psi_M) = \eta$. On the other hand, the free energy change of the subsystem may be decomposed as:

$$\Delta G^{sub} = \Delta G^W + \Delta G^R \tag{6}$$

where ΔG^W and ΔG^R corresponds to changes at each of the electrodes. ΔG^W is given by:

$$\Delta G^W = G^{M/S} - G^S \tag{7a}$$

where $G^{M/S}$ and G^S are the free energies of the M/S and S systems respectively (final and initial state). ΔG^R is in turn given by:

$$\Delta G^R = -N_{M^{z+}}\mu_M^{bulk} \tag{7b}$$

since $N_{M^{z+}}$ atoms of the bulk electrode have disappeared from the R electrode made of the bulk material M. μ_M^{bulk} is the chemical potential of bulk metal M. Using Eqs. (6) and (7a), and (7b), Eq. (5c) turns into:

$$\Delta\widetilde{G} = \left[G^{M/S} - G^S - N_{M^{z+}}\mu_M^{bulk}\right] + ze_0 N_{M^{z+}}\eta. \tag{8}$$

Defining the excess of free energy with respect to the bulk material as: $\Phi(N_{M^{z+}}) = \left[G^{M/S} - G^S - N_{M^{z+}}\mu_M^{bulk}\right]$, we get $\Delta\widetilde{G} = \Phi(N_{M^{z+}}) + ze_0 N_{M^{z+}}\eta$. Eq. (8) shows that the free energy change for the formation of the *upd* deposit is the addition of two contributions, a chemical and an electrochemical one. Depending on the chemical interaction between the M-type atoms and the substrate, $\Phi(N_{M^{z+}})$ may be positive or negative. For substrate–adsorbate interactions stronger than the bulk-M interactions we have $\left(G^{M/S} - G^S\right) < N_{M^{z+}}\mu_M^{bulk}$ or $\Phi(N_{M^{z+}}) < 0$; while the opposite will be true when the substrate–adsorbate interactions are weaker than the bulk-M ones.

Dividing Eq. (8) by $N_{M^{z+}}$, we get:

$$\frac{\Delta\widetilde{G}}{N_{M^{z+}}} = (\sigma_{exc} + ze_0\eta) \tag{9a}$$

where assuming extensive behavior, we have replaced $\Phi \approx \sigma_{exc} N_{M^{z+}}$. σ_{exc} is a parameter that represents the excess of binding energy between M and S with respect to bulk M, and in the limit of a larger monolayer deposit, it should be independent of $N_{M^{z+}}$ (extensivity). Depending on the sign and magnitude of σ_{exc}, a linear growth or decrease of $\Delta\widetilde{G}$ with $N_{M^{z+}}$ is predicted. If $\sigma_{exc} > 0$, that is, if the monolayer is less stable than the bulk material, a negative overpotential will be required to turn $\Delta\widetilde{G}$ negative and the monolayer would be deposited only at overpotentials. On the other hand, if $\sigma_{exc} < 0$, $\Delta\widetilde{G}$ may become negative for positive values of η and underpotential deposition will occur. If we set in Eq. (9a) the condition $\Delta\widetilde{G} \le 0$, we get the overpotential region for stability of the *upd* monolayer, η_{stab}:

$$\eta_{stab} \le \eta_{upd} = -\sigma_{exc}/ze_0. \tag{9b}$$

At this point it is useful to recall a concept defined by Kolb et al. [43–45] the so-called underpotential shift. This quantity, defined as the difference in the potential of the desorption peak for a layer of a metal M adsorbed on a foreign substrate S and the potential of the peak corresponding to the dissolution of the pure metal M, can be identified with the quantity η_{upd} defined above.

Going back to Eq. (9a), we can summarize:

- The *upd* phenomenon will only occur in systems with a relatively strong interaction between S and M.
- Three different thermodynamic states can be predicted on its grounds: 1) a naked electrode, 2) a deposited monolayer and 3) bulk deposition.

Of course, the existence of an *upd* bilayer is not excluded in the previous analysis. The point is that an adsorbed bilayer would have a different σ_{exc} (generally less negative than that of a monolayer) and its existence (whenever $\sigma_{exc}^{bilayer} < 0$) will be closer to the bulk deposition potential.

In the case of the formation of a full monolayer, θ_{full}, the term ΔG^{sub} in Eq. (8) contains only static and vibrational contributions. However, in the case of small clusters or 2-d islands translational contributions come also into question. Then, the most general form to write the free energy of the subsystems becomes:

$$\Delta G^{sub} = \Delta U^{static} + \Delta G^{vib} + \Delta G^{tras} \tag{10}$$

where ΔU^{static}, ΔG^{vib} and ΔG^{tras} correspond to static, vibrational and translational contributions, respectively. The first term ΔU^{static}, corresponds to the change of potential energy at $T = 0$ K calculated at the average position of the atoms and its magnitude depends on the interaction potential employed for its evaluation. In metallic systems, where the interactions are of the many-body type, the usual choices are semiempirical potentials like EAM [46,67–69], tight binding [47], and MEAM [48]. For small systems, DFT calculations [49] are becoming an option due to the increasing computational power available. Good compilations for metallic systems can be found in the reviews of Li [50] and Xiao [51]. ΔU^{static} generally delivers the largest contribution to ΔG^{sub}.

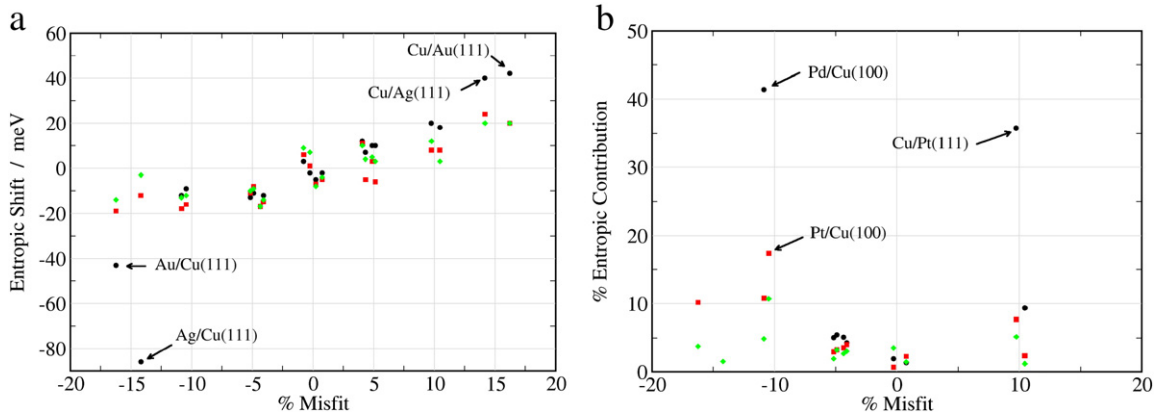

Fig. 2. a) Entropic vibrational contribution to *upd* shift at 300 K as a function of crystallographic misfit for 60 different metal systems. The latter figure result from the consideration of different metal adatom/substrate pairs taken from the set of metals {Au, Ag, Pt, Pd, and Cu} and the set of single crystal faces {(111), (100), and (110)}. b) Entropic vibrational contribution (in percent) to the free energy difference associated with underpotential shift. Only *upd* systems are considered. Black circles, red squares and green diamonds correspond to (111), (100) and (111) surfaces, respectively. The values were extracted from Table 3 of Ref. [37].

The vibrational contribution, ΔG^{vib}, may be estimated from the fluctuations of the atomic positions from their average value. For those systems where the atomic displacements from their equilibrium positions are relatively small, the energetic and entropic contributions, ΔU^{vib} and $T\Delta S^{vib}$ may be estimated from harmonic analysis. In fact, this may be a reasonable approach for pseudomorphic bimetallic systems with negligible mobility and misfit [37]. Fig. 2a shows the vibrational contribution to *upd* (*opd*) shift for 60 different pairs of systems as a function of crystallographic misfit ε. It can be observed that in general terms the entropic vibrational contribution is in the order of ± 20 mV. The system Cu/Ag(111) shown in Fig. 2a is not an *upd* system, while in the cases of Au/Cu(111) and Ag/Cu(111) it is possible that pseudomorphic deposits (as assumed to use the harmonic approximation) do not occur longer due to the large difference of lattice parameters. Fig. 2b shows the percentage of the entropic contribution to the *upd* shift, $(T|\Delta S^{vib}|) \times 100/|\Delta G^{vib}|$. It is found that for systems with small crystallographic misfit ($|\varepsilon| \leq 5$ %), the entropic contribution is lower than 5%. For systems with larger misfits ($|\varepsilon| \geq 10$ %), the entropic contribution increases considerably. However, it is possible that in the case of large positive misfits, the harmonic approximation is no longer valid, while in the case of very negative misfits, pseudomorphic deposits do not occur longer in the experimental system.

In bimetallic incommensurate systems characterized by a large misfit and high adatom diffusivity, the harmonic approach may no longer be valid because of the significant anharmonic nature of the frequency modes. In these cases, ΔU^{vib} and ΔS^{vib} may be calculated via the Fourier transform of the autocorrelation function and the application of the 2PT model mentioned above [40–42]. Fig. 3 shows ΔU^{vib} and $T\Delta S^{vib}$ for Pb deposition on Au(111) as a function of coverage degree ($\theta_{full} \approx 0.71$) as an example. The energetic and entropic contributions behave in a relatively complex way. While at low and intermediate coverages ($\theta < 0.55$) the entropic contribution disfavors deposition, the opposite occurs at high coverages. Remarkably, the potential energy presents a minimum at $\theta \approx 0.67$ and then starts to increase as a result of the compression of the Pb monolayer. In the case of the Pb/Au(111) system, the entropic part is about 20% of the total *upd* shift for θ_{full} and this contribution may grow up to 50% for small bidimensional clusters [40].

The translational contributions change ΔG^{tras} may be evaluated using the 2PT model. As mentioned above, this contribution is negligible at θ_{full}, but for small clusters, the entropic contribution may grow to an amount of 20% of the total entropic change [40].

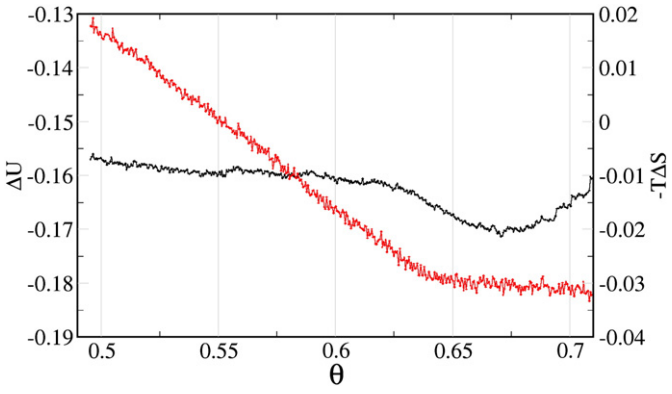

Fig. 3. Energetic ΔU (black, left scale) and entropic $-T\Delta S$ (red, right scale) components of the free energy change involved in *upd* of Pb on Au(111) as a function of Pb coverage degree θ at 300 K. All values are given in eV.

3. Thermodynamic formulation oriented to theoretical modeling of underpotential deposition including coadsorption, solvent and double layer effects

It is desirable to set up a thermodynamic formulation of *upd* enabling theoretical predictions on the basis of first principle calculations. Before formulating this modeling, we revisit the main features of the *upd* system:

1- The solid substrate/adsorbate system. This part of the system is straightforward to treat with the modern quantum mechanical tools. As we have seen above, the excess of binding energy between *M* and *S* with respect to bulk *M* gives a measure for the underpotential shift. This is a good approximation for compact adsorbates and in those cases where the work function difference between bulk *M* and bulk *S* is small. In the first case, adatoms in compact *upd* layers are largely depolarized [52], so that solvation effects should be relatively small and may be neglected. In the second case, if the work functions of *M* and *S* are similar, the shift of the potential of zero charge of the surface upon adsorbate building up will be small. If *upd* takes place at a potential where anion adsorption on the substrate is negligible due to the presence of a negative charge on the electrode surface, the same will occur with the substrate/adsorbate system and anion coadsorption effects will be minimal.

2- The solvent. As stated in the previous paragraph, this effect may be neglected in some systems but in the case of *upd* in the presence of anion coadsorption it could become very important.

3- Coadsorbed anions. These may occur in systems with large shifts in the potential of zero charge upon adsorbate formation. This is for example the case of the coadsorption of sulfate with copper species on Au(111) [53–57], as well as the coadsorption of chloride and bromide [58] with this adsorbate.
4- The electrical double layer. To the best of our knowledge, the effect of the electrical double layer (EDL) on the stability of underpotential deposits has not been addressed in the modern *upd* theories. The EDL contributes to this stability twofold: on one side, the double layer of the substrate is dismantled when the *upd* deposit forms. On the other side, it is formed again on the substrate/adsorbate system. This effect could become important in the case of *S*/*M* metal pairs showing large work function differences.

The model used represents the *upd* system taking into account the features discussed above is shown in Fig. 4. The physical picture is very close to that presented in Section 2 in Fig. 1, but it contains an important number of additional features. The electrochemical cell contains a working electrode, made of the metallic substrate *S* on which the adsorbate *M* is deposited under *upd* conditions. The reference electrode is made of the bulk metal *M* so that the potential difference measured between the two electrodes will be the underpotential shift. The system is connected to an infinite reservoirs containing solvent, anions and cations providing particles at the electrochemical (chemical) potentials μ_W^{sol}, $\tilde{\mu}_{X^-}^{sol}$, $\tilde{\mu}_{A^{a-}}^{sol}$, $\tilde{\mu}_{K^+}^{sol}$, and $\tilde{\mu}_{M^{z+}}^{sol}$, respectively. M^{z+} and A^{a-} denote species that may interact chemically with the substrate, K^+ and X^- indicate ionic species that do not adsorb and only participate building charge at the outer Helmholtz plane (OHP), together with the electronic charge located at the electrode (see zoom of interphase shown in Fig. 4b).

We make two further assumptions: first, that the contributions of M^{z+} and A^{a-} to the charge building at the OHP are negligible, that is, that their concentrations are negligible in comparison with those of the supporting electrolyte, containing K^+ and X^-; second, that as a result of coadsorption, a compound with a well defined stoichiometry is formed on the surface of *S*, say MA_n. Thus, we will write the reaction for the formation of the *upd* deposit on *S* according to:

$$\Delta kW + \Delta jK^+ + \Delta lX^- + M^{z+} + nA^{x-} + S(Q_1, solv) + \lambda e_S^- \rightleftarrows MA_n/S(Q_2, solv) \tag{11}$$

where Δj, Δk and Δl denote the change in the number of water, cationic K^+ and anionic X^- species at the substrate/adsorbate/electrolyte interphase upon formation of the *upd* deposit, λ is the number of electrons transferred for the formation of the MA_n species, and Q_1 and Q_2 denote the charge on the surface of the electrode. The term "*solv*" qualifying *S* indicates that the surface of this electrode is in contact with water molecules. In order to fulfill charge conservation the reaction taking place at the *M* electrode will be:

$$\frac{\lambda}{z}M \rightarrow \frac{\lambda}{z}M^{z+} + \lambda e_M^-. \tag{12}$$

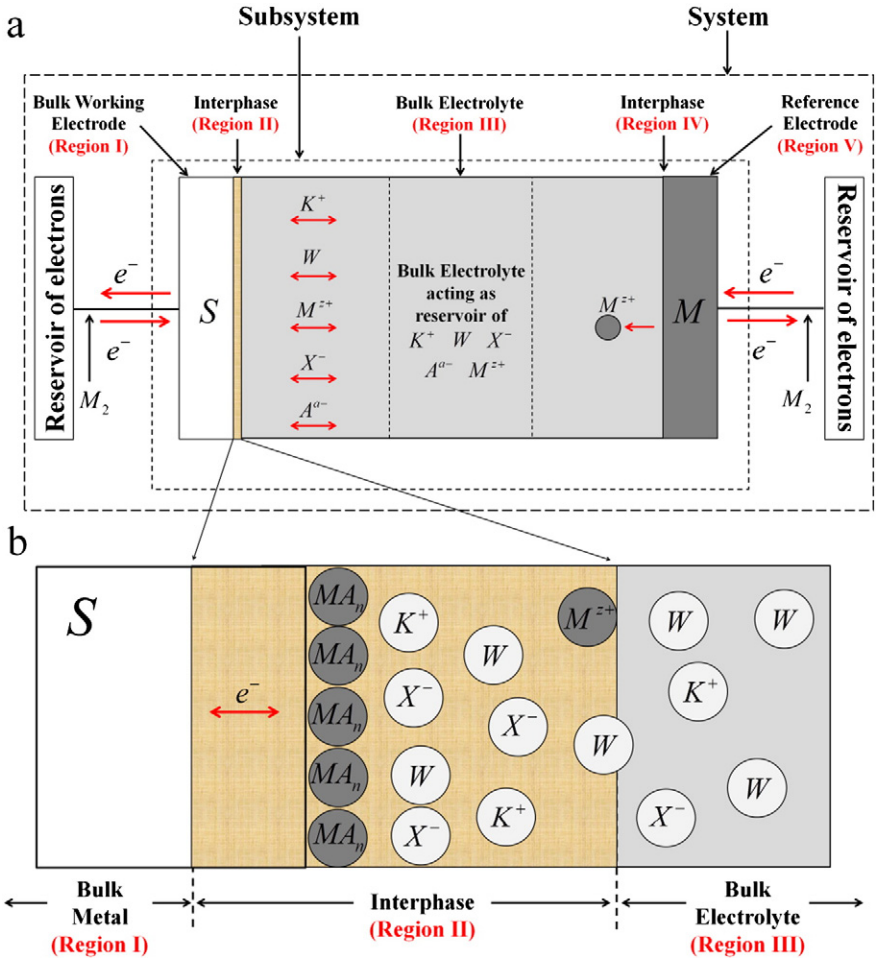

Fig. 4. a) Scheme of the electrochemical system used to evaluate underpotential shift accounting for solvent, the occurrence of anion coadsorption and electrical double layer effects. The inner dotted line encloses the subsystem containing the electrodes and the electrolyte. The subsystem is connected to two electron reservoirs and to another reservoir containing solvent *W*, the anionic X^-, A^{a-} and cationic K^+, M^{+z} species at the electrochemical potentials μ_W^{sol}, $\tilde{\mu}_{X^-}^{sol}$, $\tilde{\mu}_{A^{a-}}^{sol}$, $\tilde{\mu}_{K^+}^{sol}$ and $\tilde{\mu}_{M^{z+}}^{sol}$, respectively. b) Zoom of the interphase under consideration.

Addition of Eqs. (11) and (12) leads to:

$$\Delta kW + \Delta jK^{+} + \Delta lX^{-} + \frac{\lambda}{z}M + \left(1-\frac{\lambda}{z}\right)M^{z+} + nA^{a-} + S(Q_1, solv) + \lambda e_S^{-} \rightleftarrows MA_n/S(Q_2, solv) + \lambda e_M^{-}. \quad (13)$$

Note that in reaction (13) a number $(1-\lambda/z)$ of the M^{z+} core ions building MA_n/S must stem from the solution. This can be contrasted with the process illustrated in Fig. 1. There, we see that to get one adsorbed M^{z+} species on S, we just need one M^{z+} core ion taken from bulk M. This one-to-one relationship bears as a consequence that the *upd* shift, as calculated in Eq. (9b), is independent of the activity of M^{z+} cations in solution. This means that if the underpotential shift is measured using solutions with different activities (concentrations) of M^{z+}, always the same value should be obtained. We will see below that in the presence of specifically adsorbed anions, the situation is different.

The thermodynamic potential describing the stability of the system is:

$$\widetilde{G} = G^{sub} - N_e^S\widetilde{\mu}_e^S - N_e^M\widetilde{\mu}_e^M - N_{A^{a-}}\widetilde{\mu}_{A^{a-}}^{sol} - N_{M^{z+}}\widetilde{\mu}_{M^{z+}}^{sol} - N_{X^-}\widetilde{\mu}_{X^-}^{sol} - N_{K^+}\widetilde{\mu}_{K^+}^{sol} - N_W\mu_W^{sol} \quad (14)$$

where N_i denotes the number of i-species in the subsystem. We have added superscripts S, M and *sol* to denote the nature of the different species. The free energy is related to a surface that corresponds to a surface unit cell containing the MA_n species. The free energy change for reaction (13), according to Eq. (14) is:

$$\Delta\widetilde{G} = \Delta G^{sub} - \Delta N_e^S\widetilde{\mu}_e^S - \Delta N_e^M\widetilde{\mu}_e^M - \Delta N_{A^{a-}}\widetilde{\mu}_{A^{a-}}^{sol} - \Delta N_{M^{z+}}\widetilde{\mu}_{M^{z+}}^{sol} - \Delta N_{X^-}\widetilde{\mu}_{X^-}^{sol} - \Delta N_{K^+}\widetilde{\mu}_{K^+}^{sol} - \Delta N_W\mu_W^{sol} \quad (15)$$

where ΔG^{sub} corresponds to the change of free energy of the subsystem inscribed in the inner dashed rectangle shown in Fig. 4a. To calculate ΔG^{sub}, we divide the subsystem into five parts, as illustrated in Fig. 4a. These five parts correspond to:

I) Bulk S electrode.
II) Interphase between S (eventually M) and the solution.
III) Bulk solution.
IV) Interphase between M and the solution.
V) Bulk M electrode.

Thus, we have $\Delta G^{sub} = \Delta G^{I} + \Delta G^{II} + \Delta G^{III} + \Delta G^{IV} + \Delta G^{V}$. Let us analyze each contribution. The bulk of S remains unaltered in reaction (13), so $\Delta G^{I} = 0$. The reservoirs provide ions and solvent, so the bulk of the solution will remain unaltered, so $\Delta G^{III} = 0$. The only change on the M electrode is the disappearance of λ/z bulk M atoms, remaining its double layer unaltered. Thus, $\Delta G^{V} = -\lambda\mu_M^{bulk}/z$ and $\Delta G^{IV} = 0$. We are only left with the calculation of ΔG^{II}, that is, the free energy change of the substrate/adsorbate/solution interphase. This is a term that in the usual thermodynamic treatments is addressed as γdA, being γ the specific surface energy and A the area, and involves the formation the *upd* deposit, with the corresponding EDL, as well as the disappearance of the naked substrate/solution interface. Thus, we can write:

$$\Delta G^{sub} = \Delta G^{II} - \frac{\lambda}{z}\mu_M^{bulk} \quad (16)$$

and

$$\Delta\widetilde{G} = \Delta G^{II} - \frac{\lambda}{z}\mu_M^{bulk} - \Delta N_e^S\widetilde{\mu}_e^S - \Delta N_e^M\widetilde{\mu}_e^M - \Delta N_{A^{a-}}\widetilde{\mu}_{A^{a-}}^{sol} - \Delta N_{M^{z+}}\widetilde{\mu}_{M^{z+}}^{sol} - \Delta N_{X^-}\widetilde{\mu}_{X^-}^{sol} - \Delta N_{K^+}\widetilde{\mu}_{K^+}^{sol} - \Delta N_W\mu_W^{sol}. \quad (17)$$

Thus, we have to focus our attention on part II (interphase). With this purpose, we have to deal with the problem of calculating free energy changes for this charged interphase. Let us now consider the reactions taking place at II in terms of Eq. (11), which we split in the following set of processes (reactions), giving below each of them the free energy changes of this interphase. Fig. 5 shows schematically the thermodynamic cycle.

1. Discharging the substrate/solution interphase, taking it to the point of zero charge.

$$S(Q_1, solv) + (Q_1/e_0)e_S^{-} \rightleftarrows S(Q=0, solv) + j_{dis}K^{+} + l_{dis}X^{-} + k_{dis}W \quad (18)$$

Here, j_{dis}, l_{dis} and k_{dis} represent the number of cations, anions and water molecules leaving the interphase II during the discharge

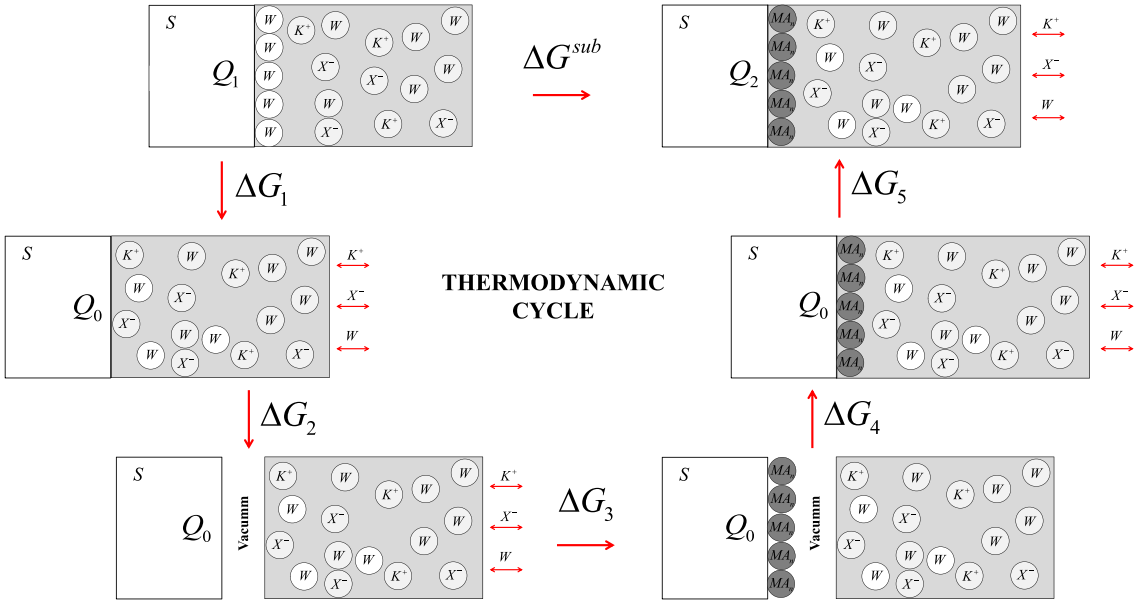

Fig. 5. Schematic picture of the thermodynamic cycle leading to reaction sequence (18),(20), (22),(24) and (26).

process. These numbers may be positive or negative, and must be calculated with a suitable model of the EDL. Negative j_{dis}, l_{dis} or k_{dis} values would mean that these species are not leaving but entering interphase II. For example, in the case of a model representing the solution side of the EDL as point charges embedded in a dielectric continuum, we would have $k_{dis} = 0$.

We denote the free energy change related to this process as:

$$\Delta G_1 = G^{S(Q=0,solv)} - G^{S(Q_1,solv)} \tag{19}$$

where $G^{S(Q_1,solv)}$ is the free energy of the charged substrate/adsorbate/electrolyte interphase and $G^{S(Q=0,solv)}$ is its free energy at the point of zero charge.

2. Desolvating the discharged substrate:

$$S(Q=0,solv) \rightleftarrows S(Q=0,vac) + j_{desolv}K^+ + l_{desolv}X^- + k_{desolv}W \tag{20}$$

where j_{desolv}, l_{desolv} and k_{desolv} represent the number of cations, anions and water molecules leaving the interphase II upon desolvation of the substrate. This process can be imagined as removing the substrate from the discharged interface, creating two new interphases: the substrate/vacuum and the vacuum/solution ones. Since the interphase is here already at the point of zero charge, the number of anions leaving/entering the interface should be equal to the number of cations doing so. Thus, we have the mass balance conditions $j_{desolv} = l_{desolv}$. We denote this free energy change as:

$$\Delta G_2 = G^{S(Q=0,vac)} + G^{sol(Q=0,vac)} - G^{S(Q_1=0,solv)} \tag{21}$$

where $G^{S(Q=0,vac)}$ is the free energy of the substrate in vacuum and $G^{sol(Q=0,vac)}$ is free energy of the solution part of the interphase exposed to vacuum, denoted by "*vac*". It must be emphasized that this desolvation energy does not involve a pure solvent, but an ionic solution.

3. Building the adsorbate on the surface on the substrate, from electrons from the bulk of the substrate and ions from the bulk the solution (or from the reference electrode):

$$(z-na)e_S^- + S(Q=0,vac) + M^{z+} + nA^{a-} \rightleftarrows MA_n/S(Q=0,vac) \tag{22}$$

with:

$$\Delta G_3 = G^{MA_n/S(Q=0,vac)} - G^{S(Q=0,vac)} \tag{23}$$

where $G^{MA_n/S(Q=0,vac)}$ and $G^{S(Q=0,vac)}$ are the free energies of the substrate/adsorbate and the substrate in vacuum, respectively. We note the solution side remains unaltered, since the ions are provided by the reservoir.

4. Solvation the discharged substrate/adsorbate surface:

$$MA_n/S(Q=0,vac) + j_{solv}K^+ + l_{solv}X^- + k_{solv}W \rightleftarrows MA_n/S(Q=0,solv) \tag{24}$$

where j_{desolv}, l_{desolv} and k_{desolv} represent the number of cations, anions and water molecules coming into interphase II due to solvation of the substrate/adsorbate surface. As in the case of Eq. (20), $j_{solv} = l_{solv}$ and we have:

$$\Delta G_4 = G^{MA_n/S(Q=0,solv)} - G^{MA_n/S(Q=0,vac)} - G^{sol(Q=0,vac)} \tag{25}$$

where $G^{MA_n/S(Q=0,solv)}$ is the free energy of the substrate/adsorbate/solution interphase at the point of zero charge.

5. Bringing the substrate/adsorbate/solution interphase from the point of zero charge to its final charged state:

$$MA_n/S(Q=0,solv) + j_{ch}K^+ + l_{ch}X^- + k_{ch}W \rightleftarrows MA_n/S(Q_2,solv) + (Q_2/e_0)e_S \tag{26}$$

Table 1
The number of particles exchanged by the subsystem in Fig. 4 with the reservoirs, according to Eqs. (11) and (12), which added yield the global reaction (13). These numbers are to be inserted in Eq. (17).

Eq.	ΔN_e^M	ΔN_e^S	$\Delta N_{A^{a-}}$	$\Delta N_{M^{z+}}$	ΔN_{X^-}	ΔN_{K^+}	ΔN_W
(18)	0	Q_1/e_0	0	0	$-l_{dis}$	$-j_{dis}$	$-k_{dis}$
(20)	0	0	0	0	$-l_{desolv}$	$-j_{desolv}$	$-k_{desolv}$
(22)	0	$z-na$	n	1	0	0	0
(24)	0	0	0	0	l_{solv}	j_{solv}	k_{solv}
(26)	0	$-Q_2/e_0$	0	0	l_{ch}	j_{ch}	k_{ch}
(12)	$-\lambda$	0	0	$-\lambda/z$	0	0	0

with:

$$\Delta G_5 = G^{MA_n/S(Q_2,solv)} - G^{MA_n/S(Q=0,solv)} \tag{27}$$

where j_{ch}, l_{ch} and k_{ch} represent the number of cations, anions and water molecules getting into interphase II during the charging process.

In Table 1 we report the corresponding number of particles exchanged with the reservoir for each of the steps.

From Table 1, we find the following equalities in relation to Eq. (13):

$$\Delta k = k_{ch} - k_{disc} + k_{solv} - k_{desolv} \tag{28}$$

$$\Delta l = l_{ch} - l_{disc} + l_{solv} - l_{desolv} \tag{29}$$

$$\Delta j = j_{ch} - j_{disc} + j_{solv} - j_{desolv}. \tag{30}$$

The previous reactions are subject to the electroneutrality condition of the interphase before and after adsorbate formation. Previous to *upd*, the surface charge of substrate Q_1 is compensated by the charge of the double layer. We thus have:

$$Q_1 = -e_0(j_{dis} - l_{dis}). \tag{31}$$

After *upd*, and according to the sequence of Eqs. (18) to (26), we have that $\lambda = Q_1/e_0 + z - na - Q_2/e_0$ electrons, one M^{z+} ion and n A^{a-} anions have flowed to the substrate/adsorbate side of interphase II. The latter event sets the condition:

$$Q_2 = Q_1 - e_0(\lambda + z - na). \tag{32}$$

On the other hand, charge balance at the substrate/adsorbate solution interphase, at the final state (rhs of Eq. (26) involves:

$$Q_2 = -e_0(j_{ch} - l_{ch}). \tag{33}$$

So, we have the following condition for λ:

$$\lambda = -j_{dis} + l_{dis} + z - na + j_{ch} - l_{ch}. \tag{34}$$

Using the previous results and Table 1, we can replace into Eq. (15) to get:

$$\Delta\widetilde{G} = \Delta G^{sub} + \lambda\left(\widetilde{\mu}_e^M - \widetilde{\mu}_e^S\right) - n\widetilde{\mu}_{A^{a-}}^{sol} - \left(1-\frac{\lambda}{z}\right)\widetilde{\mu}_{M^{z+}}^{sol} - \Delta l\widetilde{\mu}_{X^-}^{sol} - \Delta j\widetilde{\mu}_{K^+}^{sol} - \Delta k\mu_W^{sol}. \tag{35}$$

Using the definition of electrochemical potential given in Eq. (5b), we arrive at:

$$\begin{aligned}\Delta\widetilde{G} = {} & G^{MA_n/S(Q=0,vac)} - G^{S(Q=0,vac)} - \frac{\lambda}{z}\mu_M^{bulk} - \left(1-\frac{\lambda}{z}\right)\mu_{M^{z+}}^{sol} - n\mu_{A^{a-}}^{sol} \\ & + \Delta G_{disch}^{S} + \Delta G_{ch}^{MA_n/S} \\ & + \Delta G_{desolv}^{S} + \Delta G_{solv}^{MA_n/S} \\ & + \lambda\left(\widetilde{\mu}_e^{M} - \widetilde{\mu}_e^{S}\right)\end{aligned} \tag{36}$$

where we have defined the following quantities:

$$\Delta G_{disch}^{S} := G^{S(Q=0,solv)} - G^{S(Q_1,solv)} - \left(-l_{disc}\mu_{X^-}^{sol} - j_{disc}\mu_{K^+}^{sol} - k_{disc}\mu_W^{sol}\right) \tag{37}$$

$$\Delta G_{ch}^{MA_n/S} := G^{MA_n/S(Q_2,solv)} - G^{MA_n/S(Q=0,solv)} - \left(l_{ch}\mu_{X^-}^{sol} + j_{ch}\mu_{K^+}^{sol} + k_{ch}\mu_W^{sol}\right) \tag{38}$$

$$\begin{aligned}\Delta G_{desolv}^{S} := {} & G^{S(Q=0,vac)} + G^{sol(Q=0,vac)} - G^{S(Q_1=0,solv)} \\ & - \left(-l_{desolv}\mu_{X^-}^{sol} - j_{desolv}\mu_{K^+}^{sol} - k_{desolv}\mu_W^{sol}\right)\end{aligned} \tag{39}$$

$$\begin{aligned}\Delta G_{solv}^{MA_n/S} := {} & G^{MA_n/S(Q=0,solv)} - G^{MA_n/S(Q=0,vac)} - G^{sol(Q=0,vac)} \\ & - \left(l_{solv}\mu_{X^-}^{sol} + j_{solv}\mu_{K^+}^{sol} + k_{solv}\mu_W^{sol}\right)\end{aligned} \tag{40}$$

where ΔG_{disch}^{S} is the free energy change corresponding to the discharging of the EDL of the substrate/solution interphase, taking it to its point of zero charge, $\Delta G_{ch}^{MA_n/S}$ is the free energy change corresponding to the charging of the EDL of the substrate/adsorbate/solution interphase, taking it from its point of zero charge to the status it has when the *upd* monolayer has been formed. $\Delta G_{solv}^{MA_n/S}$ is a solvation term corresponding to the MA_n/S surface and ΔG_{desolv}^{S} is a desolvation term corresponding to the S pristine surface (without *upd* layer).

Eq. (36) contains all the physics involved in the present problem. The first line in it refers to the formation of the 2-d deposit MA_n on S, from ions in the bulk of the solution and from electrons and ions stemming from the reference electrode. The second line contains double layer terms, accounting for the dismantlement of the double layer of the substrate and the building of the double layer of the *upd* deposit. Similarly, the third line accounts for desolvation–resolvation effects. The fourth line accounts for electronic flow from/to the two electrodes.

Since $\left(\widetilde{\mu}_e^{M} - \widetilde{\mu}_e^{S}\right) = e_0\eta$ is the potential difference that can be measured between the electrodes shown in Fig. 4a, this equation may be used to calculate the relative stability of different MA_n/S structures at different potentials. Alternatively, we can set $\Delta\widetilde{G} = 0$, and in this case the electrochemical potential difference $\left(\widetilde{\mu}_e^{M} - \widetilde{\mu}_e^{S}\right)$ will be equivalent to the desired underpotential shift η_{upd}, so we get:

$$\begin{aligned}\eta_{upd} = -\frac{1}{\lambda}\Bigg[& \left(G^{MA_n/S(Q=0,vac)} - G^{S(Q=0,vac)} - \frac{\lambda}{z}\mu_M^{bulk}\right) - n\mu_{A^{a-}}^{sol} \\ & - \left(1-\frac{\lambda}{z}\right)\mu_{M^{z+}}^{sol} + \Delta G_{rech}^{dl} + \Delta G_{resolv}\Bigg]\end{aligned} \tag{41}$$

where we have defined $\Delta G_{rech}^{dl} := \Delta G_{disch}^{S} + \Delta G_{ch}^{MA_n/S}$, a recharging free energy and $\Delta G_{resolv} := \Delta G_{desolv}^{S} + \Delta G_{solv}^{MA_n/S}$ a resolvation free energy. Eq. (41) has a twofold relevance. From the theoretical point of view, this equation allows the first-principle theoretical calculation of underpotential shifts. While the first parenthesis in Eq. (41) may be obtained precisely from DFT calculations, $\mu_{A^{a-}}^{sol}$ and $\mu_{M^{z+}}^{sol}$ involve ion solvation energies, which are subject to calculation errors of the order of a fraction of eV, making the result uncertain. A suitable alternative for their evaluation would be to use thermodynamic data, like redox potentials involving the species under consideration.

On the other hand, this equation may be also used to interpret experimental results. Assuming that the free energy contribution due to discharging/recharging of the double layer is negligible, we have, $\lambda \approx z - na$. Thus, Eq. (41) results in:

$$\begin{aligned}\eta_{upd} = -\Bigg[& \left(\frac{G^{MA_n/S(Q=0,vac)} - G^{S(Q=0,vac)}}{z-na} - \frac{1}{z}\mu_M^{bulk}\right) - \frac{n}{z-na}\mu_{A^{a-}}^{sol} \\ & - \left(\frac{1}{z-na} - \frac{1}{z}\right)\mu_{M^{z+}}^{sol} + \frac{\Delta G_{resolv}}{z-na}\Bigg].\end{aligned} \tag{42}$$

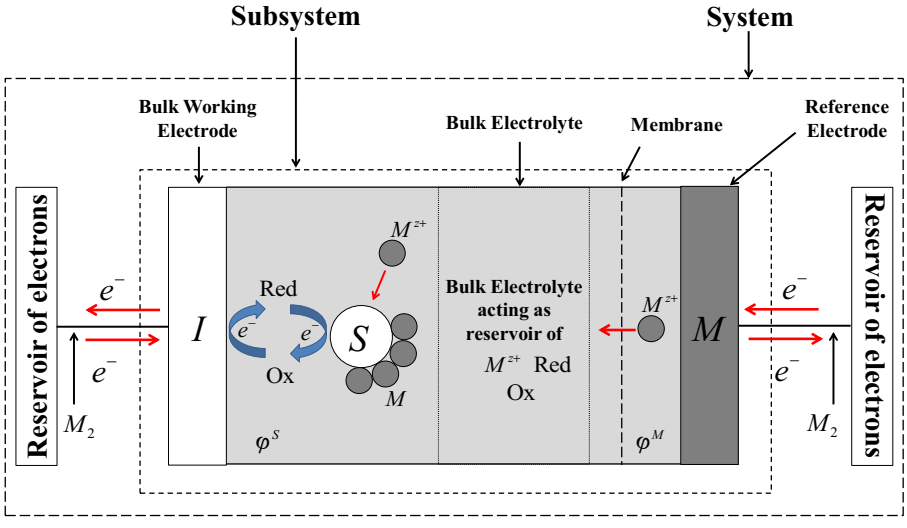

Fig. 6. Scheme of the electrochemical system used to analyze underpotential deposition on free standing nanoparticles, where a redox system used to set the potential applied to the metal nanoparticles. The broken line encloses the subsystem containing the electrodes, the nanoparticles and the electrolyte. The dotted line denotes a membrane that is permeable to all components of the system, with exception of the molecular species involved in the redox couple. The inner electrostatic potentials at both sides of the membrane is in principle different due to the presence of the redox system.

Thus, study of the dependence of the underpotential shift on the activity (and thus on the chemical potential) of the deposited cation and coadsorbed anion could yield information on the stoichiometry of the species MA_n/S being formed. In fact, we see from Eq. (42) that the following equations apply:

$$\left(\frac{\partial\eta_{upd}}{\partial\mu^{sol}_{A^{a-}}}\right)_{\mu^{sol}_{M^{z+}}} = \frac{n}{z-na} \tag{43}$$

$$\left(\frac{\partial\eta_{upd}}{\partial\mu^{sol}_{M^{z+}}}\right)_{\mu^{sol}_{A^{a-}}} = \frac{1}{z-na} - \frac{1}{z}. \tag{44}$$

Although the present restrictions do not apply strictly to their experimental data, it is worth mentioning here the work of Omar et al. [59] for Cu *upd* on Au(111) in the presence of sulfate anions. These authors observed that while the more negative *upd* peak is relatively insensitive to Cu^{+2} concentration ($\mu^{sol}_{M^{z+}}$), the more positive shows a shift $\partial\eta_{upd}/\partial c^{sol}_{M^{z+}}$ close to 30 mV/decade, indicating that $\left(\partial\eta_{upd}/\partial\mu^{sol}_{M^{z+}}\right)_{\mu^{sol}_{A^{a-}}} \approx 1/2$. Using Eq. (44) with $z = 2$ and $a = 2$, we get $n = 1/2$, in agreement with the expected $Cu(SO_4)_{1/2}$/S stoichiometry for the $\sqrt{3}\times\sqrt{3}R30^0$ structure predicted for this interphase [60,61].

4. Underpotential deposition on seed nanoparticles

A new modification of the model presented in Fig. 1 can be used to study underpotential deposition on nanoparticles freely suspended in solution. With this purpose, we add into the modeling a metal nanoparticle made of metal *S*, and a redox couple. A scheme of this system is shown in Fig. 6. In order to prevent the occurrence of unwished reactions at the *R* electrode, a membrane that is permeable to the components of the subsystem but not the chemicals associated with the redox couple is also included. The deposition reaction takes place at the left compartment. The *W* electrode is made of a chemically inert material (*I*) and is there just to allow electronic equilibrium between the redox couple and the reservoir e_W.

In the model presented in Fig. 6, cations are generated at the electrode *R* and the electrons stemming from the metal oxidation go to electron reservoir e_R. These cations go through the membrane towards the left compartment, where the deposit on the surface of a NP made of metal *S*. The electrons required for their reduction are provided by the redox couple. Another electron exchange takes place at the surface of the *I* electrode (inert surface), returning the redox system to its original state. The electrons required for this process are provided by the reservoir e_W. As the final result of this process, *M* deposition on the surface of the *S* NP occurs.

The electrochemical reaction taking place may be described as:

$$Red^u \rightarrow Ox^{u+n} + ne^- \tag{45a}$$

$$mM^{z+} + mze^- + S_p \rightarrow M_m@S_p \tag{45b}$$

which upon addition result in:

$$mM^{z+} + \left(\frac{mz}{n}\right)Red^u + S_p \rightarrow \left(\frac{mz}{n}\right)Ox^{u+n} + M_m@S_p. \tag{45c}$$

The related free energy change is:

$$\Delta\widetilde{G} = \Delta G^{sub} - \Delta N^M_e\widetilde{\mu}^M_e - \Delta N^S_e\widetilde{\mu}^S_e. \tag{46}$$

When electronic equilibrium is established at the left compartment, the electrochemical potentials of electrons at the NP, the redox system and the *I* electrode are equal. Thus, electrons from the reservoir on the left may reach the surface of the NP without the need of an electrical work. Eq. (46) looks very much like Eq. (4) and leads in a similar way to:

$$\Delta\widetilde{G} = \Delta G^{sub} + ze_0N_M\eta \tag{47}$$

where now N_M denotes the quantity of *M* atoms being deposited on the surface of the *S*-NP. We wrote "looks very much like" because the contributions in Eq. (46) and in Eq. (47) involve a number of subtleties not present in the case of *upd* on planar surfaces. The first is that the presence of the redox couple generates in principle a difference between the inner potentials of the solution in the left and the right compartments. In the case of deposition in bulk systems (Figs. 1 and 4 above), η is defined assuming the same activity of M^{z+} species in equilibrium with both electrodes, since the inner potentials of the solution are the same for both compartments. In the present case, η is defined assuming the same electrochemical potential of M^{z+} in both compartments, something that in principle would involve different activities if the inner potentials are different. This point has been discussed in detail in Reference [26]. The other difference between Eqs. (5) and (47) is that ΔG^{sub} in the former involves an infinitely large surface, while in the latter the system is finite. Even more, the system is of nanoscopic size, and the correct formalism to deal with is nanothermodynamics, as established by Hill [20]. To state these differences shortly, we can state

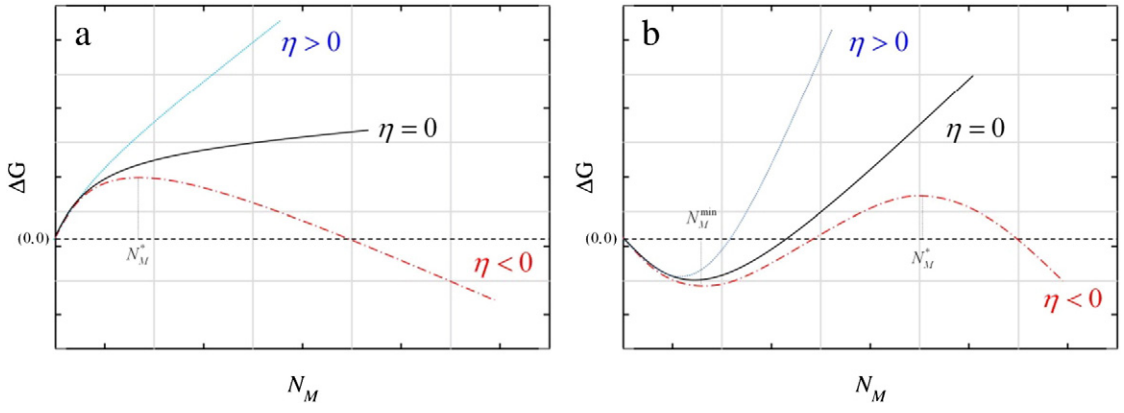

Fig. 7. Qualitative scheme of the excess Gibbs energy $\Delta\widetilde{G}$ as a function of the number of atoms N_M for the electrochemical formation of a core@shell nanostructure. a) Corresponds to a situation where the interaction of the deposited atoms with the substrate is weaker than the interaction with each other, b) opposite case of a). (Reprinted with permission from Ref. [26]).

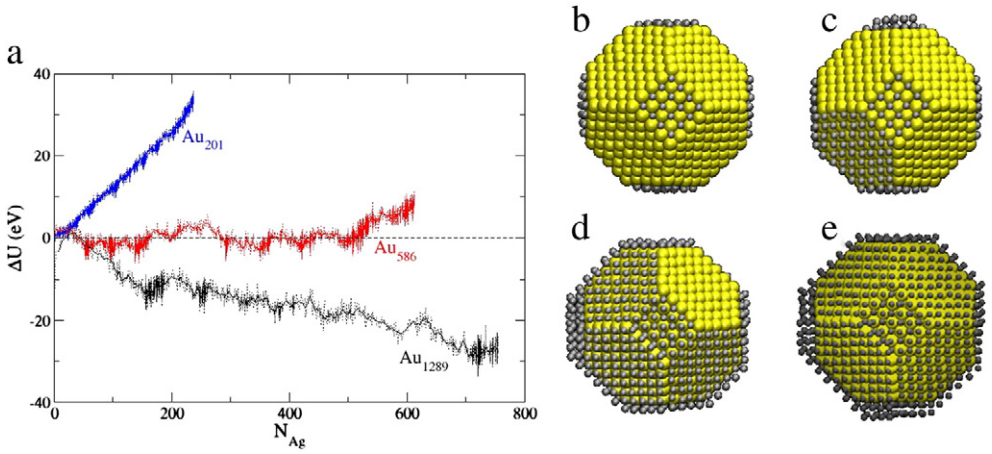

Fig. 8. a) Excess energy as a function of the number of deposited Ag atoms for Au nanoparticles of different sizes at $\eta = 0$. Representative atomic configurations taken for Au(1289) at b) $\eta = -220$mV, c) $\eta = -40$mV, d) $\eta = -20$mV, and e) $\eta = 0$mV. (Reprinted with permission from Ref. [26]).

that in Eq. (5c) ΔG^{sub} is extensive with respect to the number of adatoms, in the sense that if we multiply the number of adatoms by a constant, all the properties of the system will be scaled accordingly. In Eq. (47) this is not the case. This can easily understood with an example. Let us consider a nanoparticle where only some specific facets are covered by foreign adatoms. The binding energy per adatom (and other similar properties) will be very different from that we get when we fully cover it with adatoms of the same type. Thus, the properties of this type of systems are not extensive.

Fig. 7 shows the qualitative behavior of $\Delta\widetilde{G}$ as a function of the number of M atoms, N_M deposited on a NP for systems presenting a) *opd* and b) *upd*. In the case of *opd*, Fig. 7a, the behavior of $\Delta\widetilde{G}$ looks very much like that is usually found in the analysis of classical models of nucleation and growth. At zero or positive overpotentials, the curve shows a monotonic growth indicating that the generation of a core@shell NP is not thermodynamically spontaneous. At negative overpotentials, the curves present a maximum, corresponding to the critical nucleus size, N_M^*. For sizes smaller than N_M^*, the deposited layer is unstable and consequently dissolves, while for larger sizes it grows towards the bulk M structure. The behavior for *upd* systems, shown qualitatively in Fig. 7b, is strikingly different. There, we find a minimum in the $\Delta\widetilde{G}$ vs. N_M curve for a number of adatoms that we denote with $N_M^{\min}$. As discussed below, several minima may eventually occur. This minimum will eventually subsist at zero or slightly positive overpotentials, defining a global extremum. On the other hand, this minimum could also remain for slightly negative overpotentials, thus defining a local minimum or metastable state. This would imply the existence of core@shell nanostructures under overpotential conditions where bulk-growth should occur. The height of the free energy barrier, occurring at N_M^*, depends on overpotential, and so will the lifetime of the metastable state.

According to Eq. (1), curvature effects become more important the smaller the NPs are [15–17]. As a consequence of this, the *upd* phenomenon could disappear in the limit of small particles, thus defining an *upd–opd* transition. It has been recently suggested [25] that such a transition may be estimated from the effective binding energies of adatoms at facets $g_{M/S}^{facet,eff}$ and borders $g_{M/S}^{border,eff}$ according to:

$$N_{M/S}^{facet(upd\rightarrow opd)} = \left[-\delta\frac{\left(g_{M/S}^{border,eff}-\mu_M^{bulk}\right)}{\left(g_{M/S}^{facet,eff}-\mu_M^{bulk}\right)}\right]^2 \tag{48}$$

where $\delta > 0$ is a geometrical factor that depends on the shape of the NP and $N_{M/S}^{facet(upd\rightarrow opd)}$ is the number of adatoms at which the transition occurs. Obviously, this number is linked to a certain NP size within a given geometrical family. Eq. (23) shows that the stronger the border effects, given by $(g_{M/S}^{border,eff}-\mu_M^{bulk})$ term, the larger the NP size at which the *upd–opd* transition occurs will be. On the opposite, systems with large *upd* shifts in planar surfaces, involving a large $(g_{M/S}^{faceta,eff}-\mu_M^{bulk})$ contribution, will present the *upd–opd* transition at smaller NP sizes. According to computer simulations, *upd* has been predicted to disappear for small particle sizes in the systems Au(core)/Ag(shell) [11,19,25,26] and Au(core)/Pd(shell) [21]. In the experimental field, there is evidence that *upd* may disappear for Pb and Cd deposition on Ag NPs [20–22]. Fig. 8 shows Gran Canonical Monte Carlo (GCMC) simulations for the system Au(core)@Ag(shell), where it is evident that the *upd* phenomenon disappears for cores smaller than 512 atoms. Representative snapshots of GCMC simulations, corresponding to different overpotentials, are presented on the right of the Fig. 8b–e, where selective decoration of some facets of the NP becomes evident.

5. Conclusion

The present work was focused on relevant advances in the theory of metal underpotential deposition taking place over the past 20 years. The approach was essentially thermodynamic and some conclusions were supported based on computer simulations. Underpotential methods appear as the most suited alternative to handle metal deposition at the nanoscale, especially concerning the thermodynamic control of the structures being formed on the substrate. The reason for this is that material exchange with the environment under equilibrium conditions is greatly enhanced in electrochemical systems with respect to the gas/phase counterpart. An important step forward taken in the present work is the formulation of a thermodynamic scheme to calculate from first principles the stability of *upd* phases considering coadsorption, salvation and double layer effects. Another interesting phenomenon is the fact that underpotential deposition, depending on the strength of the substrate–adsorbate interaction may vanish in the nanoscale. This underpotential–overpotential transition may be understood in terms of a curvature effect.

Although knowledge on *upd* has been improved in the last 20 years, it is still desirable to extend the theoretical formulation to include in the modeling of *upd* on nanoparticles the effect of other coadsorbed species like hydronium ions, capping agents, etc. This will require further experimental and theoretical research. Also, the inclusion of other contributions such as electrostatic (electrical double layer) effects and description of the kinetic behavior of metal deposition at the nanoscale are desirable. A suitable option would be the application of kinetic Monte Carlo techniques.

Acknowledgments

We acknowledge the CONICET PIP 11220110100992, the SECyT Universidad Nacional de Córdoba, Program BID (PICT 2012-2324), and the PME: 2006-01581 for financial support.

References

[1] M. Ratner, D. Ratner, Nanotechnology, a gentle introduction to the next big idea, Prentice Hall, Professional Technical Reference, Upper Sadle River, NJ, 2003, p. 07458.
[2] E. Herrero, L.J. Buller, H.D. Abruña, Chem. Rev. 101 (2001) 1897.
[3] V. Sudha, M.V. Sangaranarayanan, J. Chem. Sci. 117 (2005) 207.
[4] E. Budevski, G. Staikov, W.J. Lorenz, Electrochemical phase formation and growth — an introduction in the initial stages of metal deposition, VCH, Weinheim, 1996.
[5] W. Schmickler, Interfacial Electrochemistry, Oxford University Press, USA, 1996.
[6] G. Staikov, W.J. Lorenz, E. Budevski, Imaging of surfaces and interfaces, in: P.N. Ross, J. Lipkowski (Eds.), Front. Electrochem., vol. 5, Wiley-VCH, New York, 1999.
[7] R.M. Crooks, V. Chechik, B.I. Lemon III, L. Sun, L.K. Yeung, M. Zhao, Synthesis, characterization, and applications of dendrimer-encapsulated metal and semiconductor nanoparticles, in: D.L. Feldheim, C.A. Foss Jr. (Eds.), Metal nanoparticles — Synthesis, Characterization, and Applications, Marcel Dekker, Inc., 2002.
[8] F. Epron, C. Especel, G. Lafaye, P. Marécot, Multimetallic nanoparticles prepared by redox processes applied in catalysis, in: Didier Astruc (Ed.), Nanoparticles and Catalysis, Wiley VCH, 2008.
[9] M.M. Mariscal, S.A. Dassie, Recent Advances in Nanoscience, Research Signpost, Trivandrum-Kerala, India, 2007.
[10] B. Corain, G. Schmid, N. Toshima, Metal Nanocluster in Catalysis and Materials Science, Elsevier, The Netherlands, 2008.
[11] M.M. Mariscal, O.A. Oviedo, E.P.M. Leiva, Metal Clusters and Nanoalloys: From Modelling to Applications, Springer, 2012.
[12] O.A. Oviedo, E.P.M. Leiva, Modelling of metal electrodeposition at the nanoscale, in: Z.A. Niknam (Ed.), Nano-Electrochemistry: Electrochemical Synthesis Methods, Properties and Characterization Technique, Springer, 2014, (in press).
[13] P.R. Selvakannan, A. Swami, D. Srisathiyanarayanan, P.S. Shirude, R. Pasricha, A.B. Mandale, M. Sastry, Langmuir 20 (2004) 7825.
[14] M.H. Fonticelli, G. Corthey, G.A. Benitez, R.C. Salvarezza, L.J. Giovanetti, F.G. Requejo, Y.S. Shon, J. Phys. Chem. C 111 (2007) 9359.
[15] D.M. Wood, Phys. Rev. Lett. 46 (1981) 749.
[16] W.J. Plieth, J. Phys. Chem. 86 (1982) 3166.
[17] W.J. Plieth, Surf. Sci. 156 (1985) 530.
[18] N.B. Luque, L. Reinaudi, P. Serra, E.P.M. Leiva, Electrochim. Acta 54 (2009) 3011.
[19] O.A. Oviedo, E.P.M. Leiva, M.M. Mariscal, Phys. Chem. Chem. Phys. 10 (2008) 3561.
[20] T.L. Hill, Nano Lett. 1 (2001) 273.
[21] O.A. Oviedo, L. Reinaudi, M.M. Mariscal, E.P.M. Leiva, Electrochim. Acta 76 (2012) 424.
[22] F.W. Campbell, Y. Zhou, R.G. Compton, New J. Chem. 34 (2010) 187.
[23] F.W. Campbell, R.G. Compton, Int. J. Electrochem. Sci. 5 (2010) 407.
[24] Y. Zhou, N.V. Rees, R.G. Compton, ChemPhysChem 12 (2011) 2085.
[25] O.A. Oviedo, L. Reinaudi, E.P.M. Leiva, Electrochem. Commun. 21 (2012) 14.
[26] M.M. Mariscal, O.A. Oviedo, E.P.M. Leiva, J. Mater. Res. 27 (2012) 14.
[27] M.L. Personick, M.R. Langille, J. Zhang, C.A. Mirkin, Nano Lett. 11 (2011) 3394.
[28] P. Vélez, A. Cuesta, E.P.M. Leiva, V.A. Macagno, Electrochem. Commun. 25 (2012) 54.
[29] E.V. Carino, H. You Kim, G. Henkelman, R.M. Crooks, J. Am. Chem. Soc. 134 (2012) 4153.
[30] M.R. Langille, M.L. Personick, J. Zhang, C.A. Mirkin, J. Am. Chem. Soc. 134 (2012) 14542.
[31] T.T. Tran, X. Lu, J. Phys. Chem. C 115 (2011) 3638.
[32] S.R. Brankovic, J.X. Wang, R.R. Adzic, Surf. Sci. 474 (2001) L173.
[33] M.F. Mrozek, Y. Xie, M.J. Weaver, Anal. Chem. 73 (2001) 5953.
[34] S. Park, P. Yang, P. Corredor, M.J. Weaver, J. Am. Chem. Soc. 124 (2002) 2428.
[35] J. Zhang, F.H.B. Lima, M.H. Shao, K. Sasaki, J.X. Wang, J. Hanson, R.R. Adzic, J. Phys. Chem. B 109 (2005) 22701.
[36] P. Liu, X. Ge, R. Wang, H. Ma, Y. Ding, Langmuir 25 (2009) 561.
[37] O.A. Oviedo, E.P.M. Leiva, M.I. Rojas, Electrochim. Acta 51 (2006) 3526.
[38] B.E. Conway, J.C. Chacha, J. New Mater. Electrochem. Sys. 7 (2004) 231.
[39] G.R. Stafford, U. Bertocci, J. Phys. Chem. C 111 (2007) 17580.
[40] L.M. Farigliano, M.A. Villarreal, O.A. Oviedo, E.P.M. Leiva, ECS Trans. 58 (32) (2014) 3.
[41] S.-T. Lin, M. Blanco, W.A. Goddard, J. Chem. Phys. 119 (2003) 11792.
[42] S.-N. Huang, T.A. Pascal, W.A. Goddard III, P.K. Maiti, S.-T. Lin, J. Chem. Theory Comput. 7 (2011) 1893.
[43] D.M. Kolb, M. Przasnyski, H. Gerischer, J. Electroanal. Chem. 54 (1974) 25.
[44] D.M. Kolb, M. Przasnyski, H. Gerischer, Surf. Sci. 43 (1974) 662.
[45] D.M. Kolb, in: H. Gerischer, C.W. Tobias (Eds.), Adv. Electrochem. Electrochem. Eng., vol. 11, Wiley, New York, 1978, p. 125.
[46] S.M. Foiles, M.I. Baskes, M.S. Daw, Phys. Rev. B 33 (1986) 7983.
[47] F. Cleri, V. Rosato, Phys. Rev. B 48 (1993) 22.
[48] M.I. Baskes, Phys. Rev. B 46 (1992) 2727.
[49] J.P. Perdew, A. Zunger, Phys. Rev. B 23 (1981) 5048.
[50] J.H. Li, X.D. Dai, S.H. Liang, K.P. Tai, Y. Kong, B.X. Liu, Phys. Rep. 455 (2008) 1.
[51] L. Xiao, B. Tollberg, X. Hu, L. Wang, J. Chem. Phys. 124 (2006) 114309.
[52] C.G. Sanchez, S.A. Dassie, E.P.M. Leiva, Langmuir 18 (2002) 6628.
[53] Y. Nakai, M. Zei, D.M. Kolb, G. Lehmpfuhl, Ber. Bunsenges. Phys. Chem. 88 (1984) 340.
[54] N. Batina, T. Will, D.M. Kolb, Faraday Discuss. 94 (1992) 93.
[55] D.A. Huckaby, L. Blum, J. Electroanal. Chem. 315 (1991) 255.
[56] L. Blum, D.A. Huckaby, Electroanal. Chem. 375 (1994) 69.
[57] L. Blum, M. Legault, P. Turq, J. Electroanal. Chem. 379 (1994) 35.
[58] Z. Shi, S. Wu, J. Lipkowski, Electrochim. Acta 40 (1995) 9.
[59] I.H. Omar, H.J. Pauling, K. Jüttner, J. Electrochem. Soc. 140 (1993) 2188.
[60] D.A. Huckabv, L. Blum, J. Electroanal. Chem. 315 (1991) 255.
[61] L. Blum, D.A. Huckaby, in: J.W. Halley, L. Blum (Eds.), Proceedings of the Symposium on Microscopic Models of Electrode–Electrolyte Interfaces, The Electrochemical Society, Inc., Pennington, NJ., 1992.
[62] E.P.M. Leiva, Electrochim. Acta 41 (1996) 2185.
[63] O.A. Oviedo, M.M. Mariscal, E.P.M. Leiva, Phys. Chem. Chem. Phys. 12 (2010) 4580.
[64] O.A. Oviedo, M.M. Mariscal, E.P.M. Leiva, Electrochim. Acta 55 (2010) 8244.
[65] O.A. Oviedo, C.F.A. Negre, M.M. Mariscal, C.G. Sánchez, E.P.M. Leiva, Electrochem. Comm. 16 (2012) 1.
[66] M.C. Giménez, A.J. Ramirez-Pastor, E.P.M. Leiva, J. Chem. Phys. 132 (2010) 184703.
[67] M. Del Pópolo, E.P.M. Leiva, J. Electroanal. Chem. 440 (1997) 271.
[68] M. Del Pópolo, C. Sánchez, E.P.M. Leiva, Surf. Sci. 421 (1999) 59.
[69] M.I. Rojas, C.G. Sanchez, M.G. Del Pópolo, E.P.M. Leiva, Surf. Sci. 453 (2000) 225.